Computational Modeling of Microstructure and Defect Evolution In Materials

Damien Pinto, Alexander Mamayev, Duncan Burns, Jaarli Suviranta,
Matthew Frick, Daniel Coelho, Salvador Valtierra Rodriguez,
Michael Greenwood and Nikolas Provatas.
McGill University.

Phase-field (PF) and Phase-Field Crystal (PFC) Methods

Classical field theories expanded around a reference density ρ_L

$$n = \frac{\rho - \rho_L}{\rho_L}$$

$$F_H[\rho(\vec{r})] = F_{id}[\rho(\vec{r})] + F_{ex}[\rho(\vec{r})]$$

$$\frac{F_{id}[\rho(\vec{r})]}{\rho_L k_B T R^d} \approx \int \left[\frac{n(\tilde{\mathbf{r}})^2}{2} - \xi \frac{n(\tilde{\mathbf{r}})^3}{6} + \chi \frac{n(\tilde{\mathbf{r}})^4}{12} \right] d\tilde{\mathbf{r}}$$

$$\frac{F_{ex}[\rho(\vec{r})]}{\rho_L k_B T R^d} \approx -\frac{1}{2} \int n(\tilde{\mathbf{r}}) d\tilde{\mathbf{r}} \int C(|\tilde{\mathbf{r}} - \tilde{\mathbf{r}}'|) n(\tilde{\mathbf{r}}') d\tilde{\mathbf{r}}'$$

$$\frac{\partial n}{\partial t} = \nabla^2 \left(\frac{\delta \tilde{\mathcal{F}}}{\delta n} \right) + \eta$$

Microstructural formation in matter defined by dynamical evolution of n(x,t)

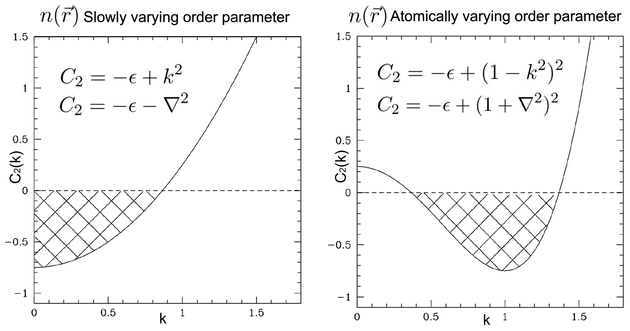

Nucleation and Growth of Vapor Bubbles with PFC (Matthew Frick)

Nucleation and growth of secondary vapor phases from Xe fission products in a polycrystalline UO_2 fuel cells.

(Right) Four FCC grains seeded with a particular amount of solute (Xe fission product). A center-cut through the axis of crystal rotation are shown at two times. Green lines denote grain boundaries and slices perpendicular to these boundaries are shown on the right.

- (Top) Nucleation and growth of several vapor pockets, some of which begin to impinge upon one another at various depths.
- (Bottom) Late time bubble coarsening. Vapor phases have grown, impinged, and in some cases completely span the thickness of the material, which leads to a known failure mechanism in nuclear materials.

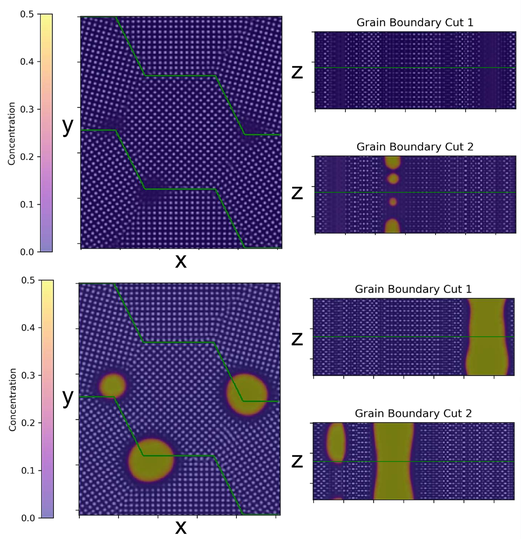

Rapid Solidification Kinetics with PFC (Duncan Burns, Martin Grant)

1)

Evolution Snapshots

1) Introduce kinetic energy
2) Atomic density amplitude changes
3) Melting Zones emerge
4) Recrystallization

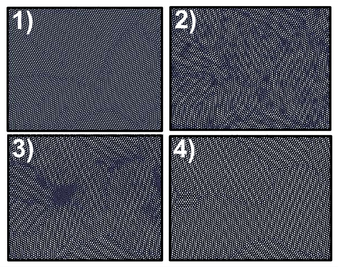

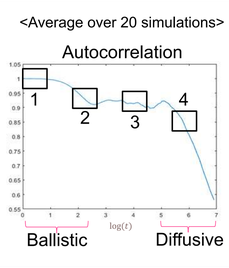

2)

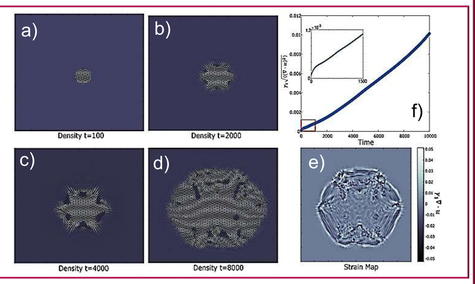

1) Gaussian distributed kinetic energy is introduced onto a polycrystal, mimicking a laser. Energy is converted into fluctuations of the average density at lattice sites. Such perturbations scatter and collect at grain boundaries, favoring the transition to a liquid phase. As energy dissipates, liquid pools recrystallize.

2) Rapid solidification regime where interface instabilities compete with vacancy diffusion. a-c) an initially circular seed of the equilibrium crystalline phase expands dendritically into an undercooled melt. As growth advances, defects (dislocations and liquid pools) become incorporated into the bulk solid as seen in d). The defects contribute to the non-linear evolution of the internal crystal strain as shown in e). f) shows the corresponding strain map snapshot to d), revealing the dendritic-like structure of fossilized defects.

Discontinuous Precipitation Reactions with PFC (Alex Mamayev)

The control of precipitate size is vital to understand strengthening mechanisms in metals. We are investigating the atomic mechanisms involved in discontinuous precipitation at grain boundaries in two-component alloys using PFC, to expand the classical theories of this phenomenon.

Classical driving forces inducing motion

$$\Delta F = RT \left[x_\alpha \ln\left(\frac{x'_\alpha}{x_\alpha}\right) + (1 - x_\alpha) \ln\left(\frac{1 - x'_\alpha}{1 - x_\alpha}\right) \right] + \frac{2\sigma V_m}{\lambda}$$

Chemical Component — Surface Component

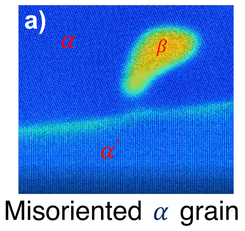

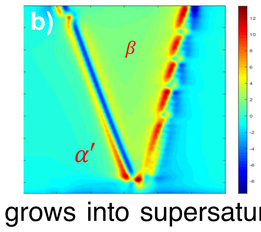

a) Misoriented α grain grows into supersaturated α' grain leaving behind lamellar β precipitates.
b) Strain fields along the edge of a fully developed lamellar precipitate growing in α' .

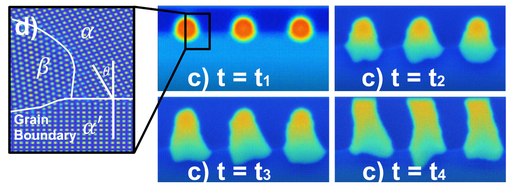

c) Overlaid density and composition fields of growing precipitates, cooler colours mean less solute. **d)** Density field around a precipitate demonstrating the crystal structure of the phases as well as the misorientation between α and α' denoted θ.

Dendritic Growth in Turbine Blades With PF (Salvador Valtierra)

Primary and secondary dendrite branching. Comparison of a 2D simulation and an experiments cut for 3 misoriented grains.

Primary and secondary branching observed in a 3D simulation. Comparison with 2D reveals in-plane grain interactions.

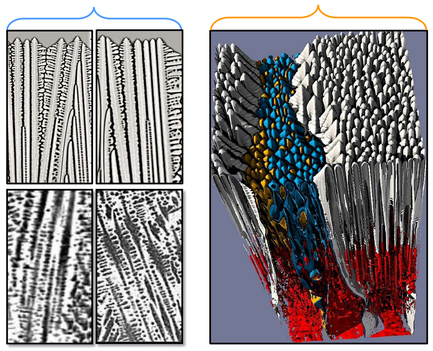

Experimental and thermo-kinetic data are employed to quantitatively determine the PF parameters to study a stainless steel, similar in composition to AISI 309L used in turbine blades by our partner Hydro-Québec.

- Length of cell-dendritic regions is directly controlled by the thermal gradient (G) and solid-liquid front speed (V).
- Experimental microstructural measurements show a mean intra-branching spacing of approximately 20.7 μm, close to simulated spacings of 18.35 μm.
- Strong side-branching is notably observed in inter-dendritic regions (grain boundaries) and increases with grain boundary mis-orientations.
- Simulations agree with the experimental solidification data.

Accelerating PF Modelling With Machine Learning (Damien Pinto)

(Right) Downward growth of crystal dendrites during solidification of a binary alloy simulated using Phase Field (PF) modeling with adaptive mesh refinement on 8 cores (bottom) and a Convolutional Long-Short Term Memory (CLSTM) neural network (top). Time steps dt = 1.6×10^{-6} s.

The CLSTM spans the same evolution time (21000 dt) but in approximately 2 orders of magnitude less computational wall time, while preserving the correct feature progression as the PF model:

- Front Velocity
- Solute pool formation
- Concentration gradients
- Side-branch emergence at correct periodicity (inset)

(t_n : time step from which CLSTM begins predicting time-evolution
dt: Time step size of PF modeling simulation)

Predictions of Directional Growth by a CLSTM Vs. PF

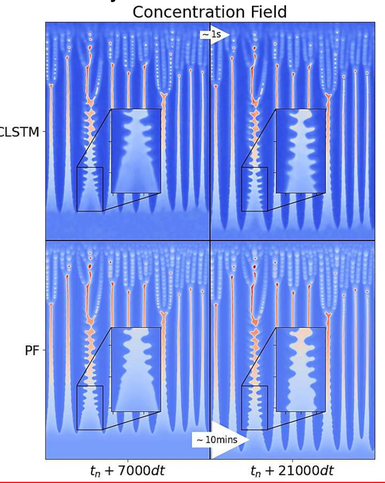

Stress Effects in Rapid Solidification with PFC (Jaarli Suviranta)

Stress-induced defects are of paramount importance in rapidly solidified materials. We model these within the PFC framework, which naturally incorporates elasto-plasticity.

(Right) Defects form between growing grains in aluminium. (Left) Grain orientations change continuously as neighboring grains stress each other during growth.

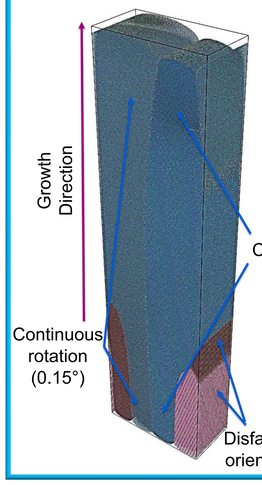

- Aluminum solidifies rapidly in simulated laser-melted pool.
- Randomly oriented grains compete to grow the fastest.
- Defects form in crystal structures as the front advances.
- Grains rotate continuously in response to each other.

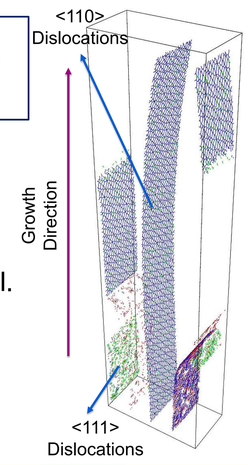

Multicomponent of Interstitial Lattices with PFC (Daniel Coelho)

1): Single crystal coexistence with liquid simulated with a two-component interstitial PFC model in 2D. B atoms (solute) site at interstitial sites of a triangular crystal lattice of A atoms (host).

2): Typical BCC/multi-component carbide (FCC) phase interfaces from TEM image of a $(TaC)_{0.9}$ alloy (adapted from Wei et.al. 2022).

- Concentration gradients
- Correlation functions -- interaction between i, j atoms $(i, j = A, B, C, \ldots)$
- Interstitial alloys (e.g. Fe-C, Ta-C)
- Crystal structure (solid) transformations
- Solid solution strengthening
- Intermetallic compounds (e.g. TaC_x, Fe_3C)

3): Polycrystal grain boundaries simulated with a 2-component interstitial PFC model in 2D.